Available online at www.sciencedirect.com
SCIENCE DIRECT®
International Journal of Solids and Structures 42 (2005) 1355–1379
INTERNATIONAL JOURNAL OF SOLIDS and STRUCTURES
www.elsevier.com/locate/ijsolstr

Compressive response of open-cell foams. Part I: Morphology and elastic properties

L. Gong, S. Kyriakides *, W.-Y. Jang

Research Center for Mechanics of Solids, Structures and Materials, The University of Texas at Austin, WRW 110, Austin, TX 78712, USA

Received 29 June 2004; received in revised form 16 July 2004
Available online 18 September 2004

Abstract

This study is concerned with the understanding and modeling of the compressive response of open cell foams. The response starts with a nearly linear elastic regime which terminates into a limit load followed by an extensive load plateau. The plateau, which is responsible for the excellent energy absorption capacity of foams, is followed by a second stiff branch. Results from polyester urethane open cell foams with relative densities of about 0.025 are used to illustrate this behavior using experiments coupled with several levels of modeling. The experiments include characterization of the microstructure and the properties of the base material and measurement of the compressive response of the foams of various cell sizes.

A sequence of models for predicting the complete response of such foam is developed. The foam is idealized to be periodic using the space-filling Kelvin cell assigned the major geometric characteristics found in the foams tested. The cells are elongated in the rise direction, the ligaments are assumed to be straight, to have Plateau border cross-sections and nonuniform cross-sectional area distribution. The ligaments are modeled as shear-deformable extensional beams and the base material is assumed to be linearly elastic. Prediction of the initial elastic moduli are addressed in Part I. Closed form expressions for the material constants are presented as well as results using a FE model of the characteristic cell. Comparison between measurements and predictions is very favorable. The paper finishes with results from a limited parametric study of the elastic moduli. The results demonstrate that inclusion of the geometric complexities mentioned above is essential for successful prediction of the moduli of such foams. The nonlinear parts of the response including the foam crushing behavior are addressed in Part II.

Keywords: Open cell foams; Mechanical response; Morphology; Elastic properties

* Corresponding author. Tel.: +1 5124714167; fax: +1 5124715500.
E-mail address: skk@mail.utexas.edu (S. Kyriakides).

0020-7683/$ - see front matter © 2004 Elsevier Ltd. All rights reserved.
doi:10.1016/j.ijsolstr.2004.07.023

1. Introduction

Cellular microstructure is widely used by both nature and man to conserve materials and reduce weight in materials and structures. Natural applications include most woods, cork, stalks of plants, cancellous bone, sponge, coral, etc. The manufacture and use of synthetic cellular materials which mimic nature have seen an enormous increase in the last 40 years where today they may be one of the most widely used man-made classes of materials. These include space filling structural *foams* and their two-dimensional counterparts *honeycombs*. In these materials, performance is optimized primarily by geometric arrangement of the solid in space to form an interconnected network of cells with nearly straight edges. The cell faces are often open (*open cells*) and other times covered by plates or membranes (*closed cells*). Synthetic cellular materials can be made from all major material categories including metals, polymers, ceramics, paper and carbon. The most commonly used honeycombs have hexagonal cells although other cell shapes (circular, rectangular, triangular) are also available. By contrast, foams consist of polyhedra which typically have 10–17 faces.

A major advantage of cellular materials is that they can be manufactured with relative ease to varying densities which are only a few percent (~2–10% but can be as low as 0.3%) of the density of the base material. They have excellent energy absorption characteristics and are widely used for shock mitigation in vehicles of all types, in packaging and in cushioning. They are also widely used as cores in sandwich plates and shells which is one of the most effective weight saving design options for structures in a variety of applications. The advent of carbon and ceramic foams has recently enabled the use of such construction in high temperature applications in jet engine nacelles and rocket nozzles.

The design and use of this class of materials require that the microstructure be related to the properties (mechanical, thermal, acoustic, etc.). Gibson and Ashby's book (1997) gives an excellent review of the state of the art as well as basic information on cellular materials. Hilyard and Cunningham (1994), Weaire and Hutzler (1999), a recent MRS Bulletin (2003) and the book by Ashby et al. (2000) provide articles on a broad range of foam issues from manufacturing to application.

The present two part series of papers deals with the mechanical behavior of open cell foams. Fig. 1 shows the compressive stress (σ = force/undeformed area) -displacement (δ/H) response of a polymeric open cell foam which is characteristic of most cellular materials. It consists of a nearly linear elastic regime which terminates into a limit load. This is followed by a load plateau which extends to an average strain of about 50% followed by a second stiff branch. The polymer in question is a viscoelastic solid so on unloading a hysteresis is traced. The hysteresis loop is initially open at zero load but with time, as the material relaxes,

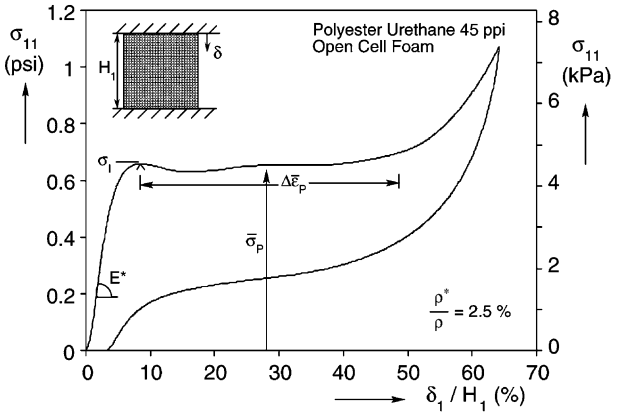

Fig. 1. Compressive stress–displacement response characteristic of many foams.

it closes at the origin. The load plateau is responsible for the excellent energy absorption characteristics of such foams while the recovery of deformation makes them useful in cushioning.

The characteristic shape of the loading part of the response in Fig. 1 is found in most foams of both open and closed cell types. The task at hand is to relate the deformation history of the microstructure to the main variables of this response $\{E^*, \sigma_I, \bar{\sigma}_P, \Delta\bar{\varepsilon}_P\}$. It was recognized early on that the initial stiff branch of the response involves stable elastic deformation of the microstructure. This has led to an evolution of micromechanical models of increasingly more representative nature (e.g., Gent and Thomas, 1963; Gibson and Ashby, 1982; Choi and Lakes, 1995; Warren and Kraynik, 1997; Zhu et al., 1997). Simultaneously it was observed that honeycomb, crushed in plane, exhibits very similar response to foams (e.g., Patel and Finnie, 1970; Gibson et al., 1982). Because of the simplicity afforded by its 2-D microstructure, honeycomb was used extensively as a model material to elucidate the events past the first load peak. It was clearly demonstrated that the load peak corresponds to the onset of an instability which localizes and then spreads at a nearly constant load through the specimen (Shaw and Sata, 1966; Shim and Stronge, 1986; Klintworth and Stronge, 1988; Gibson et al., 1989; Papka and Kyriakides, 1994, 1998a,b,c; Triantafyllidis and Schraad, 1998). When the whole specimen is crushed (densified) the response becomes stable again. The elastic properties and the onset of the instability can be found from characteristic cell type analyses (some using simple strength of materials models). The plateau stress and its extent require more extensive finite size models which simulate the whole test from the elastic regime to densification.

The work on honeycombs has clearly shown that modeling of the response and accurate prediction of the variables of interest require: (1) Accurate representation of the geometry of the microstructure and (2) measurement and appropriate modeling of the constitutive behavior of the base material. The present study will be guided by these requirements. In Part I results from crushing experiments on polymeric open cell foams are presented and discussed. Following is characterization of the morphology of the microstructure and aspects of the constitutive behavior of the polymer base material. An idealized model is then developed and used to establish the elastic properties of the foam using several models with increasingly more representative features. Part II deals with the modeling of the onset of instability and of the postbuckling response associated with the load plateau.

2. Foam processing and morphology

The foams analyzed in this study are polyester urethane foams manufactured by *Foamex*. They were selected because they could be obtained in a variety of cell sizes in approximately the same material system. Results from five such foams with nominal cell sizes of 3, 10, 20, 45 and 100 pores per inch (ppi) will be considered. Following is an outline of the processing followed by a study of the morphology of the foams.

2.1. Processing

The basic ingredients of flexible urethane foams of the type considered in this study are ester resin (or polyol), diisocyanate, water, catalysts and surfactants (e.g., Artavia and Macosko, 1994; Priester and Turner, 1994; Foamex, 2003). These are introduced in a controlled manner in a mixer (in some cases air is added). CO_2 released from the isocyanate–water reaction forms bubbles which expand. Simultaneously, the chemical reaction which is highly exothermic produces a cross-linked polyester urethane network (gelling reaction). The pressure in the gas bubbles causes expansion resulting in volume increase of 40–50 times. The packing of the bubbles is decided during the expansion. When their volume fraction exceeds about 75% their walls start to intersect forming polyhedra. Fully developed polyhedra consist of a framework of interconnected slender ligaments which serve as channels of flow. The sides of the polyhedra are covered with thin membranes. Eventually the polymer starts to gel and at this time the gas bubbles rupture the thin

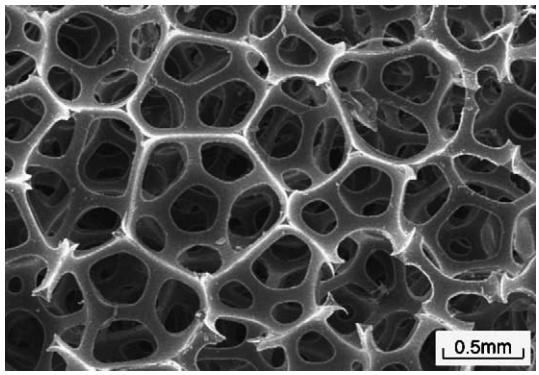

Fig. 2. Micrograph showing cellular microstructure of a polyester urethane foam (100 ppi).

membranes opening the cells. What is left behind is illustrated in the micrograph in Fig. 2. The timing of the cell opening is crucial in getting structurally sound materials. The catalysts help adjust the foaming chemistry and time while the surfactants help mix incompatible components in the reaction and stabilize bubble expansion. The process is relatively fast lasting between 2 and 4 min. Cell size is determined by the surfactant type and amount as well as by the mixing speed and back pressure. In some of the foams the membranes are removed by mechanical shock while in others they are removed chemically. The cross-section of the ligaments is in the form of a three cusp hypocycloid known as Plateau border (1873) and the most common junction of ligaments has four members.

2.2. Cell morphology

The *Foamex*-SIF foams analyzed are polyester urethane material systems with approximately the following composition by weight: ester resin 100 parts, diisocyanate 43–50 parts, water 3.3–3.8 parts, surfactant 1–4 parts and catalysts 0.5–2.0 parts. Their nominal cell sizes were: 3, 10, 20, 45 and 100 pores per inch (ppi). Measured cell sizes appear in Table 1 ($\bar{h}_1$ is the average cell height in the rise direction based on 20–30 measurements). This type of foam is used in filtering where a high degree of uniformity and cleanliness of the cellular microstructure (or low *polydispersity*, Kraynik, 2003) is a requirement. Included in Table 1 are the maximum and minimum heights of cells measured in each foam. As a measure of polydispersity we have chosen the ratio of one standard deviation (Σ_{h_1}) of the measured values of h_1 to the average value of the measurements. The results in Table 1 show that, with one exception, this ratio

Table 1
Geometric and material parameters of reticulated polyester urethane foams analyzed

Foam ppi	$\bar{h}_1$ in (mm)	$\bar{h}_1$ | min – max in (mm)	$\frac{\Sigma_{h_1}}{\bar{h}_1}$	λ	$\frac{\rho^*}{\rho}$ (%)	$\frac{E_1^*}{E}$ (%)	$\frac{E_2^*}{E}$ (%)	σ_I psi (kPa)	$\bar{\sigma}_P$ psi (kPa)	$\Delta\bar{\varepsilon}_P$ (%)
3	0.365 (9.27)	0.201–0.427 (5.11–10.8)	0.122	1.432	2.18	0.227	0.0701	0.584 (4.03)	0.56 (3.9)	46
10	0.292 (7.42)	0.263–0.328 (6.68–8.33)	0.066	1.360	2.47	0.181	0.0707	0.65 (4.48)	0.62 (4.3)	44
20	0.170 (4.32)	0.153–0.185 (3.9–4.7)	0.050	1.281	2.36	0.200	–	0.71 (4.9)	0.69 (4.8)	47
45	0.0714 (1.81)	0.064–0.084 (1.6–2.1)	0.070	1.256	2.44	0.215	0.103	0.84 (5.8)	0.83 (5.7)	47
100	0.0302 (0.767)	0.025–0.034 (0.64–0.86)	0.079	1.233	2.82	0.229	0.128	0.92 (6.3)	0.90 (6.2)	45

$\rho \approx 0.0432\,\text{lb/in.}^3$ ($1.19\,\text{g/cm}^3$); $E \approx 10$ ksi (69 MPa); $\nu = 0.49$; $\Sigma_{h_1} \equiv$ standard deviation.

is less than 0.1 which confirms that the microstructure is unusually uniform for polyester urethane foams. This is achieved by the amount and type of surfactant used, as well as by the mixer speed and back pressure.

The five foams had relative densities (ρ^*/ρ) ranging between approximately 2.2–2.8% (Table 1); in other words their relative densities have the same order of magnitude. This, coupled with the relatively uniform cell sizes in each foam, indicated that the microstructure might scale with cell size. This was indeed found to be true, at least to first order, from comparisons of the microstructures of the 5 foams analyzed using optical and scanning electron microscopy. An example of such a comparison is shown in Fig. 3 where optical micrographs of three foams [(a) 3 ppi, (b) 10 ppi and (c) 45 ppi], enlarged by different amounts to make the cells approximately the same size, are shown. The microstructures are seen to be similar supporting its scaling with cell size.

The cell morphology was found to be in general disordered consisting of a variety of cell shapes. Matzke, in his classic work (1946) in which he characterized 600 soap bubbles in a foam he assembled, reported a great variety of irregular polyhedra. We conducted a similar study which involved 30 cells extracted from the 3 ppi foam. The results are summarized in Table 2. Polyhedra with 9–17 faces were found with the average number of faces being 13.7. This matches exactly the corresponding average number reported by Matzke. The most numerous (7) polyhedra were 14-sided with 15 and 13 sides following. Once again the trend matches that reported by Matzke. The faces had 3–7 edges with the average number being 4.94 edges per face. This compares to Matzke's average of 5.12 edges per face. We attribute this difference to the much larger number of samples in Matzke's study as well as to differences in connectivity between a low density soap foam and polymeric foams.

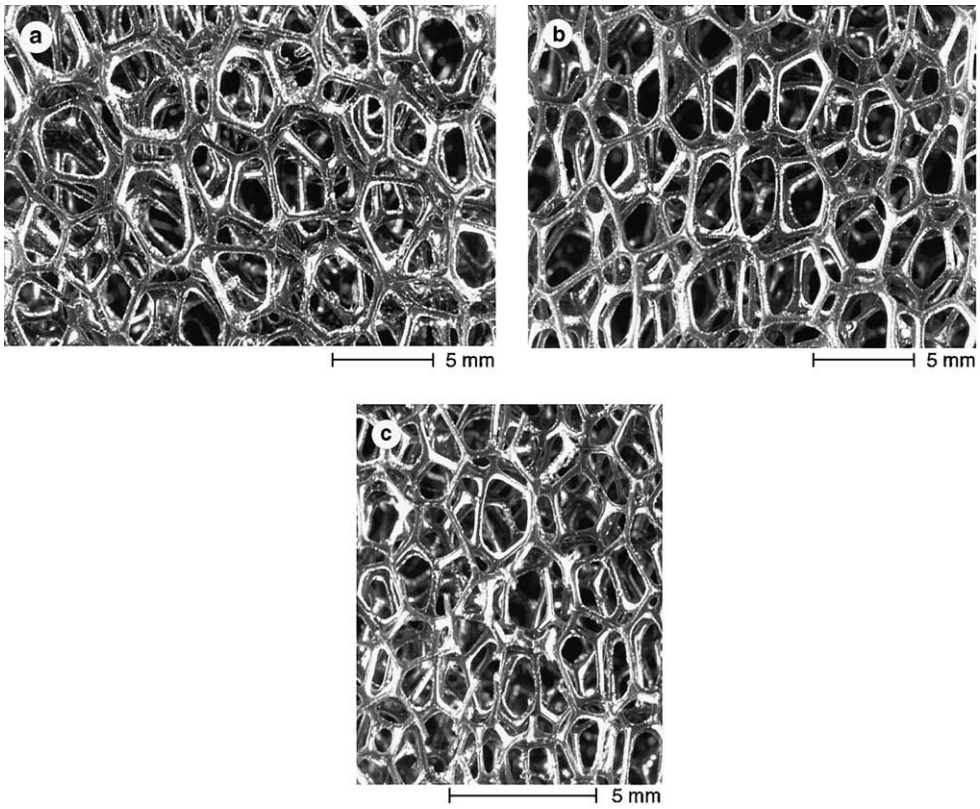

Fig. 3. Photomicrographs showing side views of three different size cells: (a) 3 ppi, (b) 10 ppi and (c) 45 ppi.

Table 2
Geometric characteristics of cells of a 3 ppi polyester urethane foam

Polyester urethane open cell foam				Number of edges				
No.	$\bar{h}_1$ (in.)	λ	Number of faces	3	4	5	6	7
1	0.360	1.443	13	0	1	10	2	0
2	0.361	1.243	15	0	3	7	4	1
3	0.395	1.506	14	0	4	7	2	1
4	0.409	1.560	17	0	3	10	3	1
5	0.349	1.475	14	0	4	4	6	0
6	0.400	1.452	16	2	4	5	4	1
7	0.405	1.427	14	0	3	8	3	0
8	0.391	1.484	16	0	2	8	6	0
9	0.406	1.468	16	0	3	8	3	2
10	0.427	1.546	17	1	3	8	4	1
11	0.357	1.264	15	1	2	9	3	0
12	0.397	1.586	12	0	0	12	0	0
13	0.427	1.793	15	1	4	5	5	0
14	0.334	1.487	11	0	2	8	1	0
15	0.394	1.634	12	0	5	5	2	0
16	0.366	1.510	14	0	5	5	4	0
17	0.365	1.498	10	1	4	5	0	0
18	0.201	1.065	9	0	7	2	0	0
19	0.334	1.292	14	1	2	9	2	0
20	0.351	1.614	11	0	2	8	1	0
21	0.355	1.121	14	0	2	7	5	0
22	0.352	1.455	13	0	4	6	3	0
23	0.410	1.599	17	1	7	5	3	1
24	0.368	1.505	13	0	6	5	2	0
25	0.320	1.285	13	0	4	8	1	0
26	0.318	1.296	14	0	2	8	4	0
27	0.375	1.340	15	0	6	3	6	0
28	0.321	1.285	12	1	2	7	2	0
29	0.378	1.360	15	0	3	8	4	0
30	0.326	1.369	11	0	4	4	3	0
Average	0.365	1.432	13.7	4.94 edges/face				

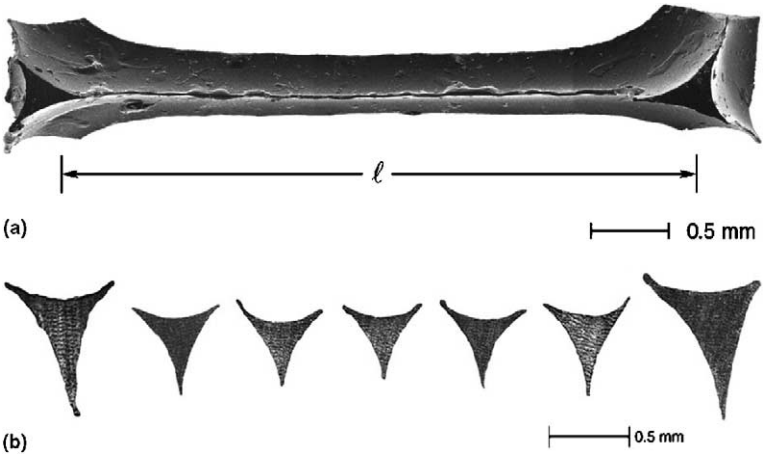

Fig. 4. (a) A typical foam ligament and (b) cross-sections taken along its length.

The cells of Matzke's foam did not have any preferential orientation because of the special way the soap foam was assembled (constructed manually bubble-by-bubble). The foams analyzed in this study exhibited some anisotropy in the shapes of the cells in the form of elongation along the rise direction (see Fig. 3). The anisotropy was quantified for each foam by comparing the maximum height of cells to their lateral dimensions ($\lambda = h_1/h_2$; e.g., see Table 2). The mean values of the λ's of the five foams analyzed are reported in Table 1. They vary from about 1.43 to 1.23 with the values decreasing with cell size. (Huber and Gibson (1988) reported similar values of anisotropy for a group of polyurethane foams.)

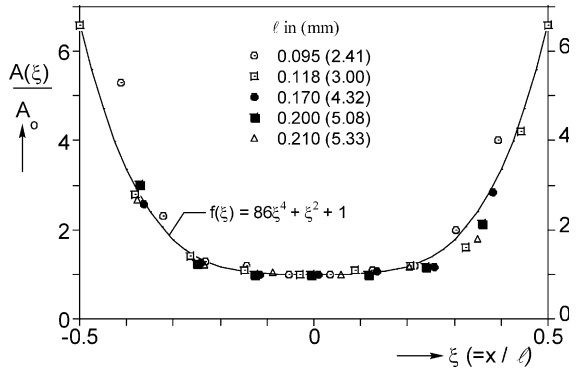

Fig. 5. Measured variation of ligament cross-sectional area along their length fitted with function $f(\xi)$.

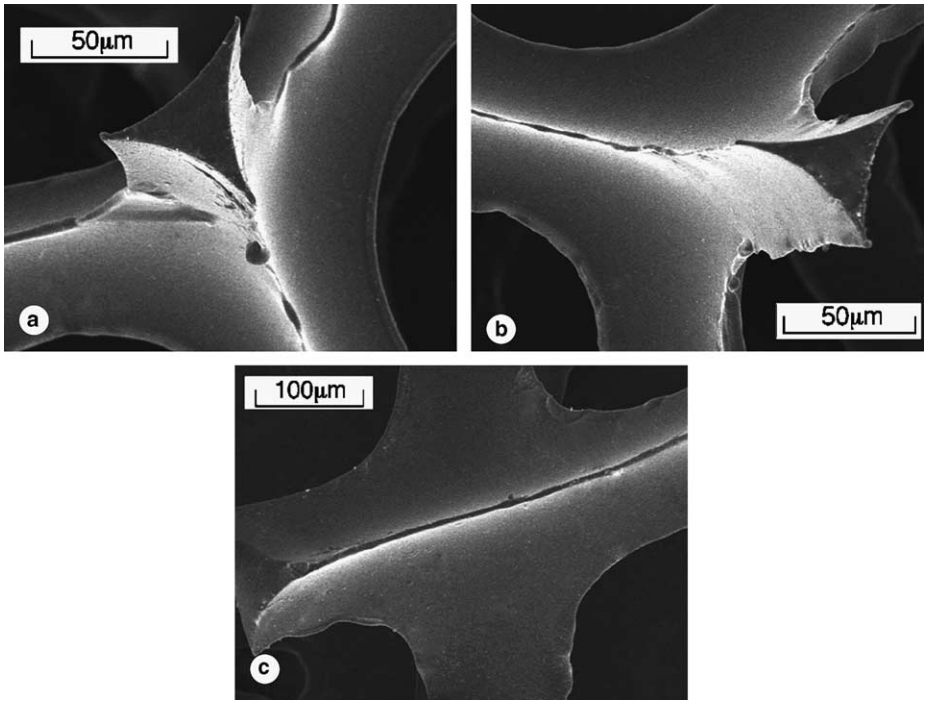

Fig. 6. Micrographs showing three four-ligament foam nodes. (a) and (b) 100 ppi, and (c) 45 ppi.

The nearly linear members which form the edges of the polyhedra, often called struts, will be referred to as ligaments. Ligaments were surgically extracted from the three coarser foams and used to establish their geometry. Fig. 4a shows a SEM micrograph of a typical ligament. Several ligaments were potted in a wax compound and sectioned along the length using a microtome. Fig. 4b shows a set of cross-sections obtained in this manner. The ligaments are nearly linear and have the characteristic three-cusp hypocycloid cross-section (*Plateau borders*). The area of the cross-section increases as the junctions (nodes) with other ligaments on either end are approached. Measurements of length and area distribution were performed and a sample of the results is presented in Fig. 5. The cross-sectional area $A(\xi)$ normalized by the value at mid-span, A_0, is plotted against the normalized length. The data were fitted with the following symmetric function:

$$A(\xi) = A_0 f(\xi) = A_0(a\xi^4 + b\xi^2 + 1), \quad \xi = x/\ell. \tag{1}$$

The constants $a = 86$ and $b = 1$ were found to yield a good fit of the data.

Fig. 6 shows micrographs of three ligament nodes taken from 100 and 45 ppi foams. They are all junctions of four ligaments which are by far the most commonly occurring ones. The nodes are seen to have smooth curved surfaces while simultaneously they are significant concentrations of material. This and the nonuniformity of the ligament cross-sections will have to be appropriately represented in modeling. Representation of the ligaments as simple uniform cross-section Bernoulli–Euler beams, adopted in most modeling efforts to date, is an oversimplification appropriate only for foams of the lowest relative densities ($\rho^*/\rho \sim 0.1\%$ or less, Kraynik, 2003).

3. Foam compressive response

Compression tests in the rise and transverse directions were conducted on each of the five foams used in the study. The tests were performed between parallel rigid platens with ground surfaces, under constant displacement rates. For the four smaller cell foams the specimens were approximately 5.5 in. cubes. For the 3 ppi foam the specimen was 6 in. tall by 12 in. square. The general characteristics of the σ–δ responses (rise direction) are similar to the one shown in Fig. 1. Fig. 7a shows the loading part of the responses of the five foams measured at a displacement rate of $\dot{\delta}/H = 7.5 \times 10^{-3}\ \mathrm{s}^{-1}$ (H = height of the specimen). As we observed earlier, the microstructure scales with the relative density. Since the relative density did not vary significantly in these foams, all aspects of the major characteristics of the five responses are similar. The major parameters of the responses are summarized in Table 1 and are seen to be of similar order of

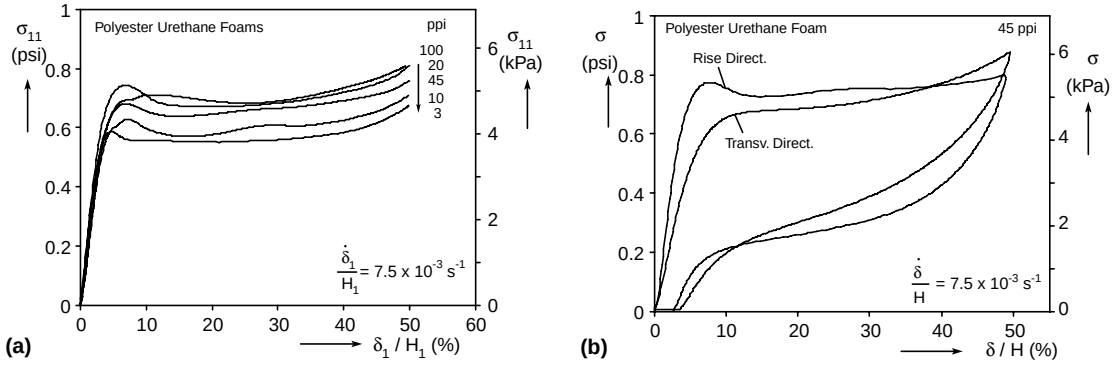

Fig. 7. (a) Comparison of rise direction compressive stress–displacement responses from foams of five cell sizes. (b) Comparison of rise and transverse direction compressive responses of 45 ppi foam.

magnitude. Differences are partly due to the relatively small variations in relative density but also to differences in the anisotropy which was found to get reduced with cell size.

The cell anisotropy causes a difference between the compressive response in the rise direction (x_1) and the one corresponding to a direction normal to it (say, x_2; transverse direction). The two responses measured in the case of the 45 ppi foam are compared in Fig. 7b. The initial modulus of the transverse response is smaller by about a factor of two (see Table 1). In addition, no load maximum is recorded and the extent of the stress plateau is shorter. Fig. 8a shows the loading part of transverse direction responses measured in four of our foams. The general trends are similar to those of the 45 ppi foam (see similar results in Fig. 2a of Huber and Gibson, 1988). The initial moduli measured in these responses are listed in Table 1 under E_2^*. More on the differences between the rise and transverse directions responses will be discussed in Part II of this series in the light of calculated results.

The mechanical properties of the foam polymer depend on the rate of loading (viscoelastic behavior). This reflects also on the compressive response of the foam. Fig. 8b shows a set of rise direction responses measured at displacement rates spanning four decades. As the rate increases the initial modulus stiffens, the load maximum increases and the whole stress plateau moves to a higher stress level. Clearly, a complete modeling of the foam requires a viscoelastic characterization of the polymer.

The elastomeric polymer also exhibits Mullins' effect (1948, 1969) which implies that the material response in the first load cycle is stiffer from subsequent cycles. Fig. 9a shows how this affects the compressive response of the foam. Shown are results from six load–unload cycles with a 5 min relaxation time between each cycle. The first cycle produces the highest initial modulus and load plateau. The second cycle exhibits a significant drop in the plateau stress while subsequently the reduction per cycle is relatively small. By the sixth cycle the material has essentially been stabilized and the responses repeat. We found that the material recovers fully after a wait of at least 48 h and the highest response is repeated. All test results that will be analyzed in this study are from fully rested foams.

Some foam chemists believe that the polymer flow resulting from the foaming process may cause preferential alignment of the long molecules of the material along the ligaments. These characteristics may not be easily achievable in bulk material. Thus, it is preferable that the mechanical properties of the polymer be measured directly from foam ligaments. This is a relatively difficult task because of the small sizes and the small loads involved and because of the relatively large strains that the ligaments must be stretched to. A small microscope testing stage, suitably modified, was used to tests ligaments from the 3 ppi foam.

The overall lengths of such ligaments are of the order of 0.12 in. (3 mm) and the load required is of the order of 20 g. The stage was equipped with a 500 g load cell and a miniature LVDT for measuring the

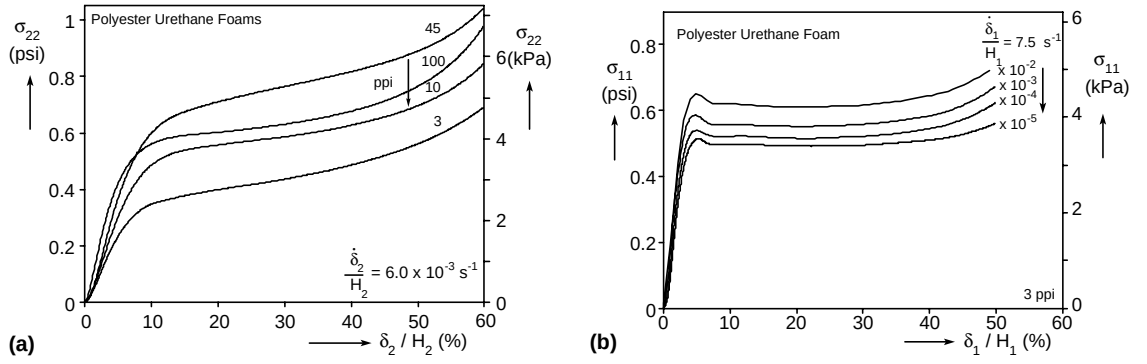

Fig. 8. (a) Comparison of transverse direction compressive stress–displacement responses from foams of four cell sizes. (b) Effect of crushing rate to compressive response of 3 ppi foam.

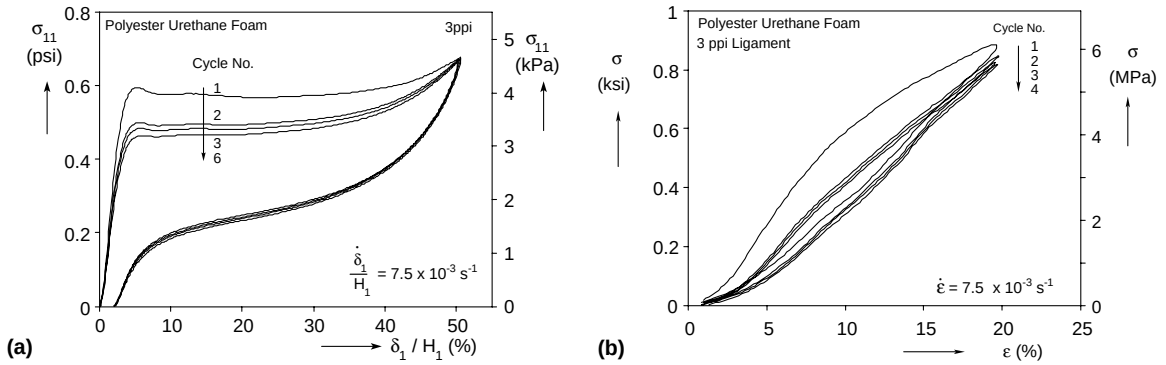

Fig. 9. (a) Compressive stress–displacement responses of 3 ppi foam (5 min rest time allowed between each load cycle). (b) Uniaxial stress–strain responses measured in single ligament (5 min rest time allowed between each load cycle).

displacement. Closed loop control was added to it so that it can run at selected rates either in load or displacement control. The nodes of the ligament were bonded to two small plates which were then clamped in the device. The ligaments were tested at different displacement rates.

Fig. 9b shows a set of load–unload stress–strain results up to a strain of about 20% from a test at a strain rate of $\dot{\varepsilon} = 7.5 \times 10^{-3}\ \mathrm{s}^{-1}$. The material is rubber-like and exhibits Mullins' effect in the first loading cycle but subsequently the response stabilizes. In this strain range, after the first cycle the material is almost linearly elastic. The slender hysteresis loops traced are mainly due to rate dependence.

The small size of the ligaments, the nonuniform and special shape of their cross-section, small initial curvature in the ligaments, difficulties in clamping the ends, and uncertainty about the exact size of the test section all contribute uncertainties to these measurements. They are thus to be considered of qualitative value. Furthermore, it is not known to what extent the mechanical properties of the four foams with smaller cells differ from the one tested.

4. Kelvin cell foam model

Efforts to model foam mechanical behavior are numerous although most are limited to the prediction of just the initial elastic constants (e.g., elastic modulus, Poisson's ratio and shear modulus). The most representative models assume some cellular microstructure (usually regular), treat the ligaments as beam columns, and use elementary strength of materials to evaluate the deformation of representative microsections. Early examples of such models include Gent and Thomas (1963) who used a cubical cell limited to just axial deformations; Ko (1965) used a cell microstructure motivated by hexagonal packing of bubbles and calculated the properties; Menges and Knipschild (1975) used a part of a cell to show that both bending and membrane deformation affect the properties; Gibson and Ashby (1982, 1997) used a cubical cell in which ligaments bend to get the correct order of magnitude dependence of the elastic constants on the relative density (see also Choi and Lakes, 1995).

The aim of the present effort is to model all major aspects of the compressive response of open cell foams seen in Fig. 1. The geometry will be idealized to be periodic by adopting the regular, 14-sided polyhedron of Lord Kelvin shown in Fig. 10 (Thompson and Lord Kelvin, 1887) which will be referred to as the *Kelvin cell*. The cell is space filling and consists of 6 squares and 8 hexagons with all edges being of the same length (ℓ). In this case the cell dimension is $h = 2\sqrt{2}\ell$. In the analyses that follow an additional simplification will be made by neglecting the material rate dependence and the small nonlinearity observed in the uniaxial tests

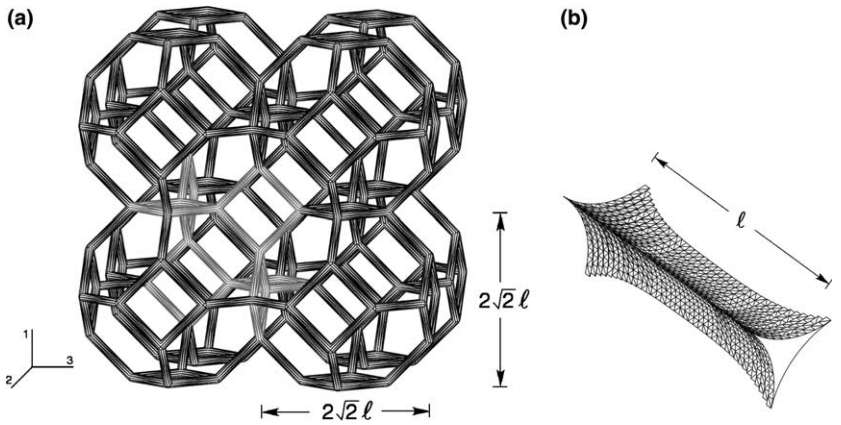

Fig. 10. (a) Cluster of 14-sided Kelvin cells. (b) Geometry of foam ligaments.

on ligaments. The material will be assumed to be linearly elastic with modulus E and Poisson's ratio v. All foams tested will be assumed to be made of the same material with the two material constants coming from best estimates based on the measurements made on the 3 ppi ligaments.

Prediction of elastic constants of Kelvin cell foams have been performed amongst others by Dement'ev and Tarakanov (1970a,b), Warren and Kraynik (1997), Zhu et al. (1997) and Pradel (1998). The ligaments were considered as Bernoulli–Euler (B–E) beams of various cross-sections (squares, circles, equilateral triangles, Plateau borders). The present study builds on these results by considering the effect of the following additional factors:

(a) Ligaments with nonuniform Plateau borders cross-sections are considered.
(b) The foam is allowed to be anisotropic.
(c) The amount of material in the nodes is represented more accurately.
(d) The effect of shear deformation is considered in beam models.

4.1. Ligament geometry

The ligaments have length ℓ and a three-cusp hypocycloid cross-section as shown in Fig. 11. The cross-section is defined by the radius r and $r_0 = r(0)$. The cross-sectional area varies along the length according to expression (1). The area and moments of inertia of this section are given by:

$$A = \left(\sqrt{3} - \frac{\pi}{2}\right) r^2 \equiv C_A r^2, \quad I_y = I_z = \frac{1}{24}\left(20\sqrt{3} - 11\pi\right) r^4 = 0.003479 r^4. \tag{2}$$

The volume of the solid is governed by the geometric variables (ℓ, r_0). They will appear in the elastic moduli through their ratio $r_0/\ell \equiv \bar{r}$.

4.2. Anisotropy

Most polymeric foams exhibit some anisotropy in the form of elongation of the cells in the rise direction. This type of anisotropy is introduced to our Kelvin cell foam in the following arbitrary but simple manner. All ligaments with a projection in the x_1-direction are elongated to $\ell/\sqrt{2}\cos\alpha$ ($\alpha \geqslant \pi/4$) while the length of

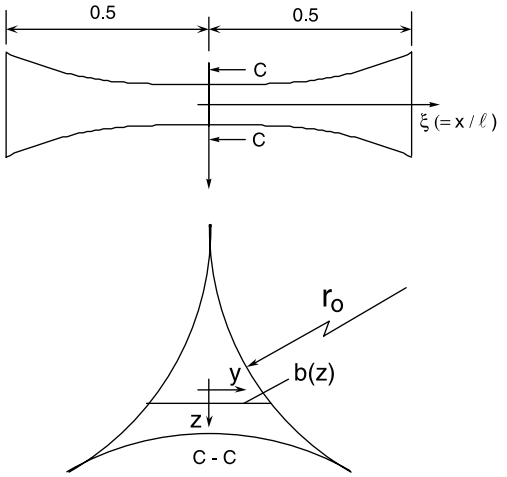

Fig. 11. Definition of geometry of foam ligaments.

ligaments in the plane normal to x_1 remains ℓ. This change makes the height of the cell $h_1 = 2\sqrt{2}\ell \tan\alpha$ while the width remains $h_2 = 2\sqrt{2}\ell$. Thus, the anisotropy parameter λ becomes

$$\lambda = \frac{h_1}{h_2} = \tan\alpha, \quad \alpha \geqslant \frac{\pi}{4}. \tag{3}$$

Fig. 12 shows the effect of this anisotropy on a cluster of Kelvin cells. The space-filling character of the cell is retained but the cells are elongated in the x_1-direction. (Dement'ev and Tarakanov (1970b) used a similar geometric distortion of the Kelvin cell to represent anisotropy.)

4.3. Volume of material at nodes

In the majority of the analytical models for elastic properties of foams mentioned above, the ligaments are represented as slender beams of length ℓ, with uniform cross-section (A). The beams rigidly connect to

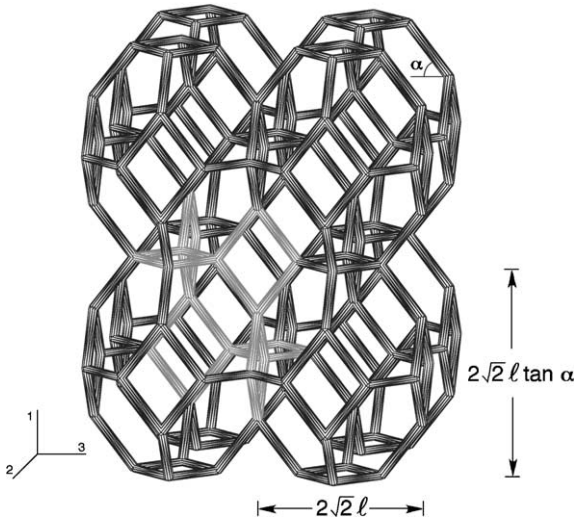

Fig. 12. Cluster of anisotropic Kelvin cells.

each other at the nodes. The volume of the beam is represented as $A\ell$. In other words, the intersection of the beams at the nodes is neglected. For our nonuniform beams this approach results in the following expression for the relative density of anisotropic Kelvin foams

$$\frac{\rho^*}{\rho} = 0.3691\left[\frac{\sqrt{2}+\cos\alpha}{3\sin\alpha}\right]\left(\frac{r_0}{\ell}\right)^2, \quad \alpha \geqslant \frac{\pi}{4}, \tag{4}$$

where the square bracket reduces to 1 for the isotropic case. The proportionality of the relative density to the second power of $r_0/\ell\,(\bar{r})$ repeats for beams of other cross-sectional shapes by replacing it with a corresponding nondimensional geometric variable.

Dement'ev and Tarakanov (1970a) avoided the problem of material distribution at the nodes by making their nodes rigid and of fixed volume. The deformable beams then connect to the surface of a node rather than to its center. The issue was also noted in Gibson and Ashby (1982) but was neglected in most of their subsequent works.

In the present study the excess material at the nodes was removed (strictly for the purposes of calculating the volume of the ligaments). This was done by cutting the ends of the beams with appropriately chosen smooth curved surfaces. Fig. 13a shows a node generated by this process. Although not a perfect match it is seen to be a good approximation of actual foam nodes like those in Fig. 6.

Taking into account the material removed results in a new relationship between the relative density and $\bar{r}$. For isotropic foams the relationship is shown graphically in Fig. 14 where it is compared to Eq. (4). For the corrected foam the relative density is proportional to $\bar{r}^{1.739}$ which makes the difference with Eq. (4) quite significant. The amount of material removed depends on the area distribution function $A(\xi)$ and must be calculated for each case separately. The case of uniform cross-section is included in Fig. 14 for comparison. In this case the correction for the volume at the nodes has a smaller effect.

Similar corrections were performed for several anisotropic cases that will be considered below. In all cases Eq. (1) was adopted for $A(\xi)$ and a powerlaw relationship (fit) was established for their relative density of the type

$$\frac{\rho^*}{\rho} = k\left(\frac{r_0}{\ell}\right)^n.$$

Results for various values of λ are listed in Table 3. Included for comparison are results for the uniform cross-section ligament. Henceforth these values will be adopted in all calculations performed on foams.

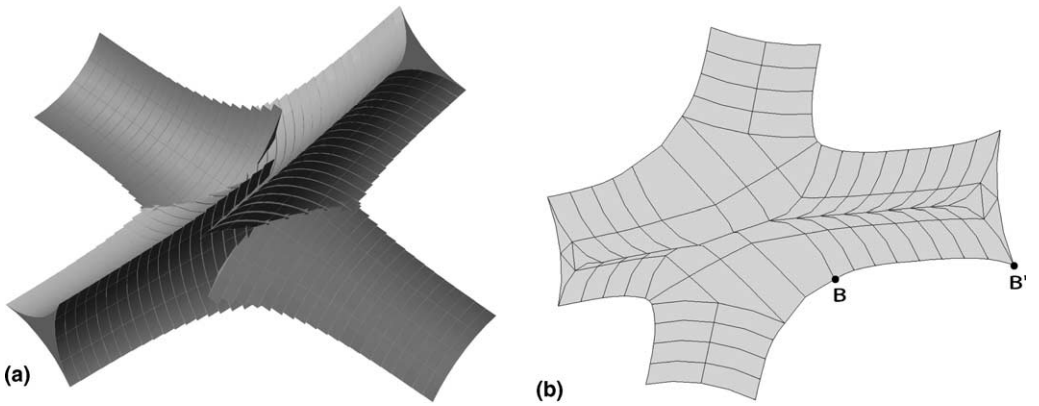

Fig. 13. (a) A Kelvin cell node of four converging beam ligaments with intersecting material removed. (b) Same node as represented by solid FEs.

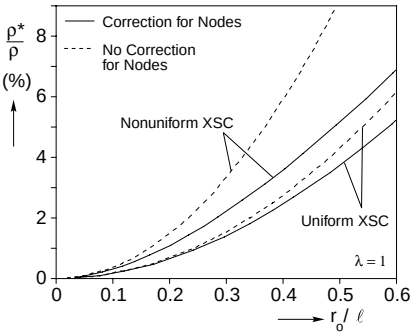

Fig. 14. Relative density vs. r_0/ℓ for Kelvin cells with and without the correction for the material at the nodes.

Table 3
Fit parameters for corrected relative density powerlaw relationship to $\bar{r}$ for variable cross-section ligaments

λ	n	k
1	1.7392	0.1803
1.1	1.7426	0.1791
1.2	1.7433	0.1637
1.3	1.7449	0.1580
1.4	1.7474	0.1350
Unif. Xsc	1.8968	0.1395

4.4. Effect of shear deformation

The foams of interest have relative density in the range of 1–5%. Ligaments of foams with even this small solid content are not very slender. As a result, when treated as beams, a Timoshenko type correction should be included for the additional deformation resulting from shear stresses. The calculations that follow are energy based and thus the correction is introduced in the strain energy due to the shear force V as follows:

$$U_s = \int_{-1/2}^{1/2} \beta \frac{V^2(\xi)}{2GA} \ell \, d\xi \quad \text{where} \quad \beta = \frac{A}{I_y^2} \int_z \frac{Q^2(z)}{b(z)} \, dz. \tag{5}$$

The second integral is over the cross-section of the ligament shown in Fig. 11 with Q being the first moment of area about the y-axis ($b(z) \equiv$ width). For this cross-section $\beta = 1.24$.

4.4.1. Beam models

The elastic moduli can be evaluated in closed form by treating the ligaments as Bernoulli–Euler beams and including the effect of axial and shear deformations. A representative microsection can be found for each loading of interest. Fig. 15 shows three examples of free-body diagrams of microsections used to establish the elastic modulus in the rise direction E_1^* and Poisson's ratio v_{12}^* (a), the bulk modulus κ^* (b), and the shear modulus G_{13}^* (c), for foams with an anisotropy $\lambda \geqslant 1$. Drawn in bold lines are the parts that are considered in each case. Figures similar to the ones in Fig. 15a and c can be drawn for uniaxial loadings in the 2- and 3-directions and for shear loading in the 1–2 and 2–3 planes (see also Zhu et al. (1997) who considered similar microsections of isotropic foams).

The axial force (N), moment (M), shear force (V), and torque (T) in each ligament are established in terms of the applied far field loads. The corresponding strain energy is then given by:

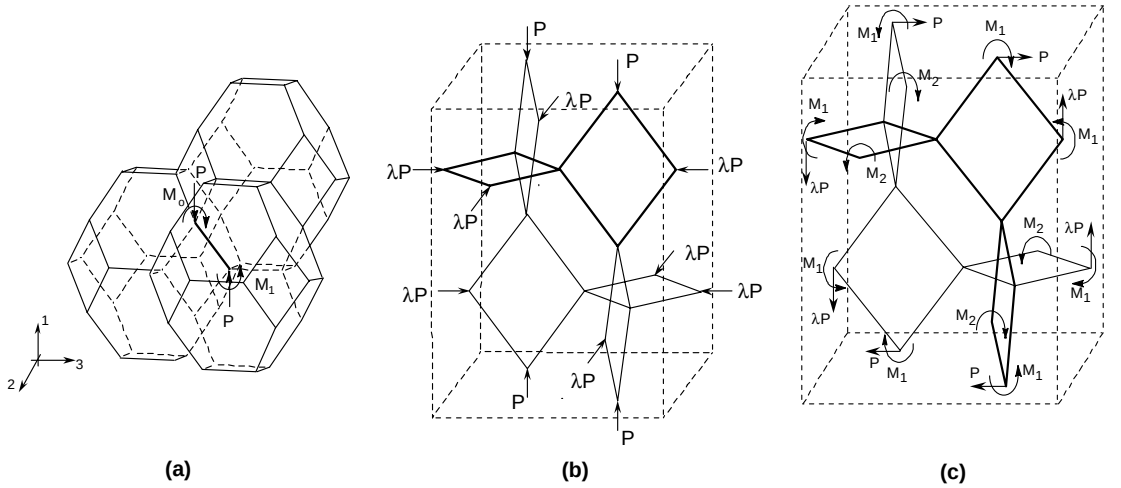

Fig. 15. Free body diagrams used to derive closed form expressions for the Kelvin cell (a) axial modulus E_1^* (b) bulk modulus and (c) shear modulus G_{13}^*.

$$U = \int_{-1/2}^{1/2} \frac{N^2(\xi)}{2EA(\xi)} \ell \, \mathrm{d}\xi + \int_{-1/2}^{1/2} \frac{M^2(\xi)}{2EI(\xi)} \ell \, \mathrm{d}\xi + \int_{-1/2}^{1/2} \beta \frac{V^2(\xi)}{2GA(\xi)} \ell \, \mathrm{d}\xi + \int_{-1/2}^{1/2} \frac{T^2(\xi)}{2GJ(\xi)} \ell \, \mathrm{d}\xi, \tag{6}$$

where the sectional properties A and I are given in Eq. (2) and E and G are the Young's and shear moduli of the linearly elastic base material. The torsional rigidity GJ based on elasticity (includes effect of warping) is $G \times 0.0021 r^4$ (Warren et al., 1997). For uniaxial compression along the x_1, x_2 and x_3 directions (Fig. 12) and for hydrostatic pressure loading, ligaments do not twist and the last term in (6) drops out.

The calculations associated with these models are somewhat lengthy but straightforward. As a result details will not be presented here. Expressions for each material constant are listed in Table 4, Panel A with definitions of auxiliary constants given in Table 5. The results in Table 4, Panel A do not include the effect of shear as shear makes the expressions too lengthy. The moduli are expressed in terms of the geometric variable $\bar{r}$, the anisotropy λ ($= \tan\alpha$), the elastic base material constants (E, ν), constants C_i which depend on the cross-sectional area distribution function $f(\xi)$, and constants D_i chosen for algebraic convenience. In case either a different cross-sectional area is selected, or a different $f(\xi)$, then constants C_i in Table 5 must be reevaluated. Because the correction for the material at the nodes depends on the anisotropy, it is not possible to present general moduli expressions for anisotropic foams in terms of the relative density as is common practice. Sample results which also include the effect of shear deformations are listed in Table 4, Panel B. These reduce to the results in Table 4, Panel A if the section correction factor β is assigned a zero value.

Results for two degenerate cases, the isotropic foam, and the isotropic foam with uniform ligament cross-section ($f = 1$) are included in the tables. Isotropy simplifies the expressions significantly. When in addition $f = 1$, comparison with results of previous works becomes possible. Zhu et al. (1997) developed expressions for $\{E^*, \nu^*, G^*, \kappa^*\}$ for general cross-section beams. Their results match the present ones for beams of general cross-section if the effect of shear, the correction for the material at the nodes, and the warping correction of the torsional rigidity are neglected. The same is true for similar results developed by Pradel (1998) (quoted in Laroussi et al., 2002). If in addition axial deformations are neglected, results in Warren and Kraynik (1997) match the present ones. The expression for E_1^* including the effect of anisotropy in Dement'ev and Tarakanov (1970b) is also in agreement with the present results under the simplifying assumptions of their model. The quantitative effect of the additional factors considered in the present models on the elastic constants will be discussed in Section 4.4.3.

Table 4
Elastic constants of anisotropic and isotropic Kelvin cell foams (Panel A); including the effect of shear deformations (Panel B)

	Anisotropic/non-uniform XSC	Isotropic/non-uniform XSC	Isotropic/uniform XSC
Panel A			
$\frac{\rho^*}{\rho}$	$k\bar{r}^n$	$k\bar{r}^n$	$k\bar{r}^n$
$\frac{E_1^*}{E}$	$\frac{C_I C_A^2 \sin\alpha \bar{r}^4}{C_1 + 2C_I C_A C_2 \sin^2\alpha \bar{r}^2}$	$\frac{C_I C_A^2 \bar{r}^4}{\sqrt{2}(C_1 + C_I C_A C_2 \bar{r}^2)}$	$\frac{12 C_I C_A^2 \bar{r}^4}{\sqrt{2}(1 + 12 C_I C_A \bar{r}^2)}$
$\frac{E_2^*}{E}, \frac{E_3^*}{E}$	$\frac{2C_I C_A^2 \cos\alpha \bar{r}^4}{\lambda[C_1(\lambda^2 + \sqrt{2}\cos\alpha) + C_I C_A C_2(2\cos^2\alpha + \sqrt{2}\cos\alpha)\bar{r}^2]}$	$\frac{C_I C_A^2 \bar{r}^4}{\sqrt{2}(C_1 + C_I C_A C_2 \bar{r}^2)}$	$\frac{12 C_I C_A^2 \bar{r}^4}{\sqrt{2}(1 + 12 C_I C_A \bar{r}^2)}$
v_{12}^*	$\frac{\lambda^2}{2}\left(\frac{C_1 - 2C_I C_A C_2 \cos^2\alpha \bar{r}^2}{C_1 + 2C_I C_A C_2 \sin^2\alpha \bar{r}^2}\right)$	$\frac{1}{2} - \left(\frac{C_I C_A C_2 \bar{r}^2}{C_1 + C_I C_A C_2 \bar{r}^2}\right)$	$\frac{1}{2} - \left(\frac{12 C_I C_A \bar{r}^2}{1 + 12 C_I C_A \bar{r}^2}\right)$
v_{21}^*	$\frac{C_1 - 2C_I C_A C_2 \cos^2\alpha \bar{r}^2}{C_1(\lambda^2 + \sqrt{2}\cos\alpha) + (2\cos^2\alpha + \sqrt{2}\cos\alpha) C_I C_A C_2 \bar{r}^2}$	$\frac{1}{2} - \left(\frac{C_I C_A C_2 \bar{r}^2}{C_1 + C_I C_A C_2 \bar{r}^2}\right)$	$\frac{1}{2} - \left(\frac{12 C_I C_A \bar{r}^2}{1 + 12 C_I C_A \bar{r}^2}\right)$
v_{23}^*	$\frac{C_1 - C_I C_A C_2 \bar{r}^2}{C_1\left(1 + \frac{\lambda^2}{\sqrt{2}\cos\alpha}\right) + (\sqrt{2}\cos\alpha + 1) C_I C_A C_2 \bar{r}^2}$	$\frac{1}{2} - \left(\frac{C_I C_A C_2 \bar{r}^2}{C_1 + C_I C_A C_2 \bar{r}^2}\right)$	$\frac{1}{2} - \left(\frac{12 C_I C_A \bar{r}^2}{1 + 12 C_I C_A \bar{r}^2}\right)$
$\frac{\kappa^*}{E}$	$\frac{C_I C_A^2 \bar{r}^4}{\frac{\cos^2 2\alpha}{\sin\alpha \cos^4\alpha} C_1 + (8\sin\alpha + 2\sqrt{2}\lambda) C_I C_A C_2 \bar{r}^2}$	$\frac{\sqrt{2} C_A}{12 C_2} \bar{r}^2$	$\frac{\sqrt{2} C_A}{12} \bar{r}^2$
$\frac{G_{12}^*}{E}, \frac{G_{13}^*}{E}$	$\frac{2\sin\alpha \cos^2\alpha C_I C_A^2 \bar{r}^4}{D_1 + 2\sqrt{2} D_2 \sin^2\alpha \cos\alpha + 2C_I C_A C_2 \bar{r}^2}$	$\frac{C_I C_A^2 \bar{r}^4}{2\sqrt{2}(D_1 + C_I C_A C_2 \bar{r}^2)}$	$\frac{C_I C_A^2 \bar{r}^4}{2\sqrt{2}\left(\frac{1}{12} + \frac{(1+\nu)}{4[C_J + 5(1+\nu)]} + C_I C_A \bar{r}^2\right)}$

$\frac{G_{23}^*}{E}$	$\frac{\cos^3\alpha C_I C_A^2 \bar{r}^4}{\lambda(D_3 + 2\sqrt{2}\cos^3\alpha C_I C_A C_2 \bar{r}^2)}$	$\frac{C_I C_A^2 \bar{r}^4}{2\sqrt{2}(D_1 + C_I C_A C_2 \bar{r}^2)}$	$\frac{C_I C_A^2 \bar{r}^4}{2\sqrt{2}\left(\frac{1}{12} + \frac{(1+v)}{4[C_J+5(1+v)]} + C_I C_A \bar{r}^2\right)}$

Panel B

$\frac{E_1^*}{E}$	$\frac{C_I C_A^2 \sin\alpha \bar{r}^4}{C_1 + 2C_I C_A C_2[\sin^2\alpha + 2\beta(1+v)\cos^2\alpha]\bar{r}^2}$	$\frac{C_I C_A^2 \bar{r}^4}{\sqrt{2}\{C_1 + C_I C_A C_2[1 + 2\beta(1+v)]\bar{r}^2\}}$	
$\frac{E_2^*}{E}$	$\frac{2C_I C_A^2 \cos\alpha \bar{r}^4}{\lambda\{C_1(\lambda^2 + \sqrt{2}\cos\alpha) + C_I C_A C_2[\sqrt{2}\cos\alpha + 2\cos^2\alpha + 2\beta(1+v)(2\sin^2\alpha + \sqrt{2}\cos\alpha)]\bar{r}^2\}}$	$\frac{C_I C_A^2 \bar{r}^4}{\sqrt{2}(C_1 + (1 + 2\beta(1+v))C_I C_A C_2 \bar{r}^2)}$	
v_{12}^*	$\frac{\lambda^2}{2}\left(\frac{C_1 - 2(1 - 2\beta(1+v))C_I C_A C_2 \cos^2\alpha \bar{r}^2}{C_1 + 2[\sin^2\alpha + 2\beta(1+v)\cos^2\alpha]C_I C_A C_2 \bar{r}^2}\right)$	$\frac{1}{2} - \left(\frac{C_I C_A C_2 \bar{r}^2}{C_1 + [1 + 2\beta(1+v)]C_I C_A C_2 \bar{r}^2}\right)$	

Table 5
Geometric and other constants which appear in elastic moduli in Table 4

	Anisotropic/non-uniform XSC	Isotropic/non-uniform XSC	Isotropic/uniform XSC
C_A	$\left(\sqrt{3}-\frac{\pi}{2}\right)$	$\left(\sqrt{3}-\frac{\pi}{2}\right)$	$\left(\sqrt{3}-\frac{\pi}{2}\right)$
C_I	$\frac{I_y}{A^2}=0.1338$	$\frac{I_y}{A^2}=0.1338$	$\frac{I_y}{A^2}=0.1338$
C_J	$\frac{J}{2I_y}=0.3018$	$\frac{J}{2I_y}=0.3018$	$\frac{J}{2I_y}=0.3018$
C_1	$\int_{-1/2}^{1/2}\frac{\xi^2 d\xi}{f(\xi)^2}=0.0168241$	$\int_{-1/2}^{1/2}\frac{\xi^2 d\xi}{f(\xi)^2}=0.0168241$	$\frac{1}{12}$
C_2	$\int_{-1/2}^{1/2}\frac{d\xi}{f(\xi)}=0.654375$	$\int_{-1/2}^{1/2}\frac{d\xi}{f(\xi)}=0.654375$	1
C_3	$\int_{-1/2}^{1/2}\frac{d\xi}{f(\xi)^2}=0.520105$	$\int_{-1/2}^{1/2}\frac{d\xi}{f(\xi)^2}=0.520105$	1
C_M	$\frac{\frac{(1+v)\cos\alpha}{C_J+(1+v)}+\frac{(1+v)(1+\lambda^2)}{2\sqrt{2}[C_J+(1+v)\lambda^2]}}{1+\frac{2\sqrt{2}(1+v)\cos\alpha}{C_J+(1+v)}+\frac{(1+v)(1+\lambda^2)}{C_J+(1+v)\lambda^2}}$	$\frac{\sqrt{2}(1+v)}{C_J+5(1+v)}$	$\frac{\sqrt{2}(1+v)}{C_J+5(1+v)}$
D_1	$C_1+\frac{(1+v)(1-2\sqrt{2}C_M)\lambda^2}{4[C_J+(1+v)\lambda^2]}C_3$	$C_1+C_3\frac{(1+v)}{4[C_J+5(1+v)]}$	$\frac{1}{12}+\frac{(1+v)}{4[C_J+5(1+v)]}$
D_2	$C_1+\frac{(1+v)(1-2\sqrt{2}C_M)}{4[C_J+(1+v)]}C_3$	$C_1+C_3\frac{(1+v)}{4[C_J+5(1+v)]}$	$\frac{1}{12}+\frac{(1+v)}{4[C_J+5(1+v)]}$
D_3	$C_1+\frac{(1+v)\cos\alpha}{4[\lambda C_J\sin\alpha+(1+v)(\sqrt{2}+\cos\alpha+\sqrt{2}\lambda^2)]}C_3$	$C_1+C_3\frac{(1+v)}{4[C_J+5(1+v)]}$	$\frac{1}{12}+\frac{(1+v)}{4[C_J+5(1+v)]}$

4.4.2. Characteristic cell and numerical models

Because of the regularity and periodicity of the microstructure chosen, most of the mechanical properties of interest can be evaluated by considering either the characteristic cell or an assembly of characteristic cells along with appropriate periodicity conditions. The characteristic cells of the isotropic and anisotropic Kelvin foams are drawn in grey in Figs. 10 and 12 respectively. The characteristic cell for the anisotropic material is shown isolated in Fig. 16. The periodicity conditions for a single unit cell can be expressed as follows: Let the three pairs of opposite bounding faces of the cell be $(\partial R_{i1}, \partial R_{i2})$ $i=1,2,3$. The displacements and rotations of points on these faces are respectively denoted by (u_{i1}, u_{i2}) and $(\theta_{i1}, \theta_{i2})$ $i=1,2,3$. The following relationships of degrees of freedom are prescribed for points on each pair of faces $(\partial R_{i1}, \partial R_{i2})$ $i=1,2,3$:

$$\begin{aligned} &u_{i1}-u_{i2}=u_{i1}^{\mathrm{ref}}-u_{i2}^{\mathrm{ref}} \quad i=1,2,3,\\ &\theta_{i1}-\theta_{i2}=0 \quad i=1,2,3, \end{aligned} \tag{7}$$

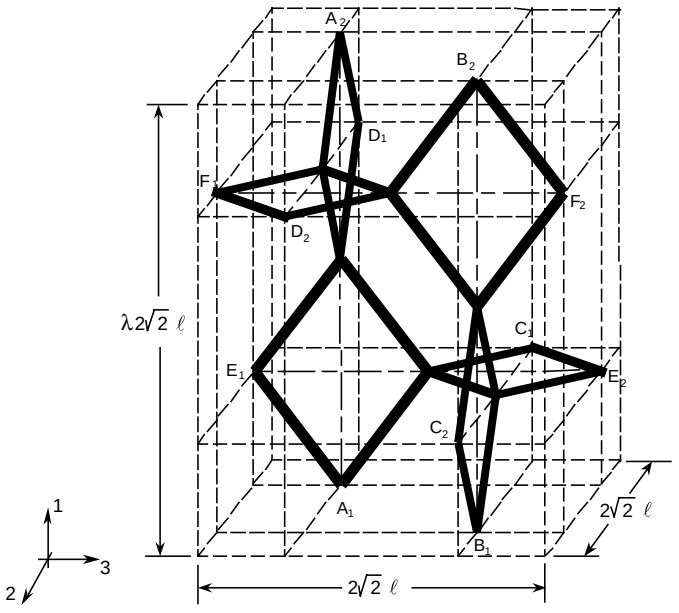

Fig. 16. The Kelvin foam characteristic cell.

where u_{ij}^{ref} are displacements of conjugate points on opposite sides chosen as reference points (e.g., (A_1, A_2), (C_1, C_2), etc.).

The characteristic cell is discretized with finite elements within the nonlinear code ABAQUS using the B32, 3-noded quadratic space beam element. Each ligament is represented by seven elements of uniform area. The area of each element is based on the symmetric function $f(\xi)$ as follows:

$$\begin{aligned} f(\xi) &= 1 \qquad 0 \leqslant |\xi| \leqslant 0.2, \\ f(\xi) &= 1.482 \quad 0.2 < |\xi| \leqslant 0.3, \\ f(\xi) &= 2.574 \quad 0.3 < |\xi| \leqslant 0.4, \\ f(\xi) &= 4.993 \quad 0.4 < |\xi| \leqslant 0.5. \end{aligned} \tag{8}$$

By using the *beam general section* feature the sectional characteristics of each beam $\{A, I_y, J\}$ are prescribed to correspond to the values listed above. In addition, the beam is made to be shear-deformable with the shear factor given in Eq. (5). The resultant model has 24 ligaments, 168 elements, 363 nodes and a total of 1980 variables.

The characteristic cell was also discretized with solid elements using C3D15V prisms and C3D27 brick elements. The philosophy behind generating the mesh was to closely match the geometry of the corresponding beam element model. As mentioned above, parts of the beams were removed in the neighborhood of the nodes in order to correctly represent the material distribution in the actual foam. The removed material depends on the relative density. For the solid model, part of the ligaments was assigned the area distribution $f(\xi)$ while the node was a smooth version of the corresponding beam node with the material removed (note that the two do not match exactly). As a result, for the relative densities considered $0.01 \leqslant \rho^*/\rho \leqslant 0.06$, the length of the ligament obeying $f(\xi)$ ranges from 0.664ℓ to 0.34ℓ.

Fig. 13b shows a 3-D model node and one ligament. Although it compares well with the beam model node shown in Fig. 13a it is not a perfect match. The part identified by B–B′ has the $f(\xi)$ area distribution. This part was modeled with 32 prism elements. Each node was modeled with 16 prisms and 8 brick

elements. The triangular prisms have 18 nodes and the bricks 27 nodes all with 3 degrees of freedom. Full integration was used for both. The full cell has 1056 elements and a total of 23,814 degrees of freedom which makes it computationally considerably more expensive than the beam model.

4.4.3. Elastic moduli predictions

The performance of the various beam models is illustrated in Fig. 17 where predictions of the elastic modulus E^* as a function of the relative density are compared for the isotropic foam. Shown are results from the inextensional Bernoulli–Euler beam (B–E), the extensional beam (B–E Exte.), the shear deformable beam, and from the FE model using B32 elements. In all cases the beam cross-section varies according to Eq. (1). The stiffest model is the simple inextensional B–E. The effect of extensionality increases with ρ^*. At relative densities of about 3% and 5% the inextensional model modulus is respectively 10% and 20% higher than the extensional model. The shear deformation plays an even more important role and can only be neglected for foams of relative densities of less than 1%. For example, at relative densities of about 3% and 5% the modulus of the shear deformable beam is only 74% and 62% respectively of the corresponding beam which precludes shear deformations. Included in the figure are results generated by the FE model. Since this beam model has the same features as the analytic extensional and shear deformable model it yields results which are in excellent agreement with the latter.

A second set of comparisons appears in Fig. 18. Here the elastic modulus and shear modulus of isotropic foams predicted by the extensional beam, the FE B32 and the 3D models are compared (all have the

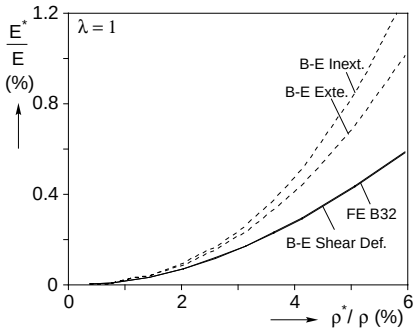

Fig. 17. Axial moduli vs. relative density calculated by different beam model assumptions.

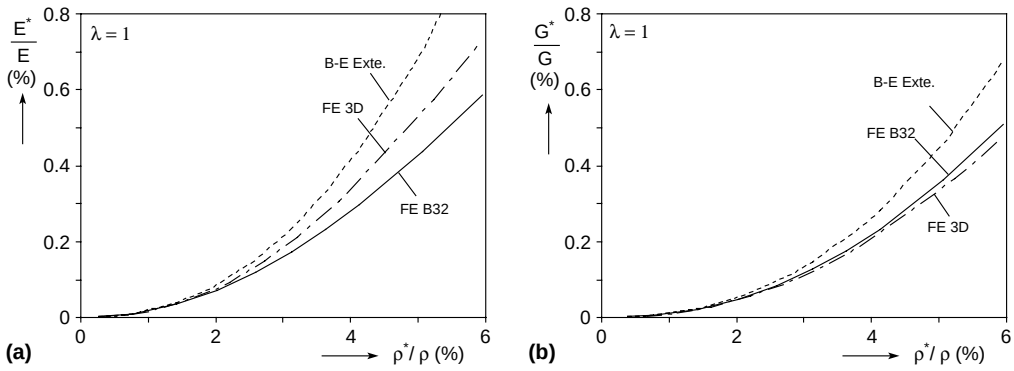

Fig. 18. Moduli vs. relative density calculated by beam models and the solid element model. (a) Axial modulus and (b) shear modulus.

corrected relative density). As pointed out above, the difference between the B–E and the FE B32 model is due to the effect of shear. The 3-D model is somewhat stiffer than the B32 model (Fig. 18a). We attribute this small difference mainly to the fact that the node geometry was somewhat different in the two models.

The FE beam model will now be used to examine the importance of some of the realistic aspects of foams introduced in this work. Fig. 19 shows the effect of the cross-sectional variation of foam ligaments on the elastic constants of the isotropic Kelvin foam. Foams with Plateau border cross-sections with uniform and nonuniform (Eq. (1)) cross-sections are compared. The effect of cross-sectional variation is very significant with the nonuniform cross-section foam being generally stiffer. For example, at a relative density of 2% the nonuniform foam Young's modulus (Fig. 19a) is nearly 69% higher than the uniform foam while at 5% relative density the difference increases to 74%. The Young's modulus to first order is governed by beam bending and, as a result, it is proportional to $\bar{r}^4$. The nonuniformity of the ligaments reduces $\bar{r}$ for a given relative density as shown in Fig. 14. However, the nonuniformity makes the ligament stiffer by about a factor of 5 (difference between C_1 and 1/12 in Table 5) which has a stronger effect than the difference in $\bar{r}$.

The difference between the two sets of results is significant but smaller for the shear modulus (Fig. 19b). The bulk modulus (Fig. 19c) is relatively unaffected by this redistribution of material primarily because it is governed by axial deformation which is less sensitive to this change. By contrast, Poisson's ratio is slightly reduced by cross-sectional nonuniformity (Fig. 19d). This stiffening effect carries through to anisotropic foams as well.

The effect of cell anisotropy in the elastic properties is illustrated in Fig. 20 where results for $\lambda = 1$, 1.2 and 1.4 are presented for foams with nonuniform cross-section. The modulus in the x_1-direction increases

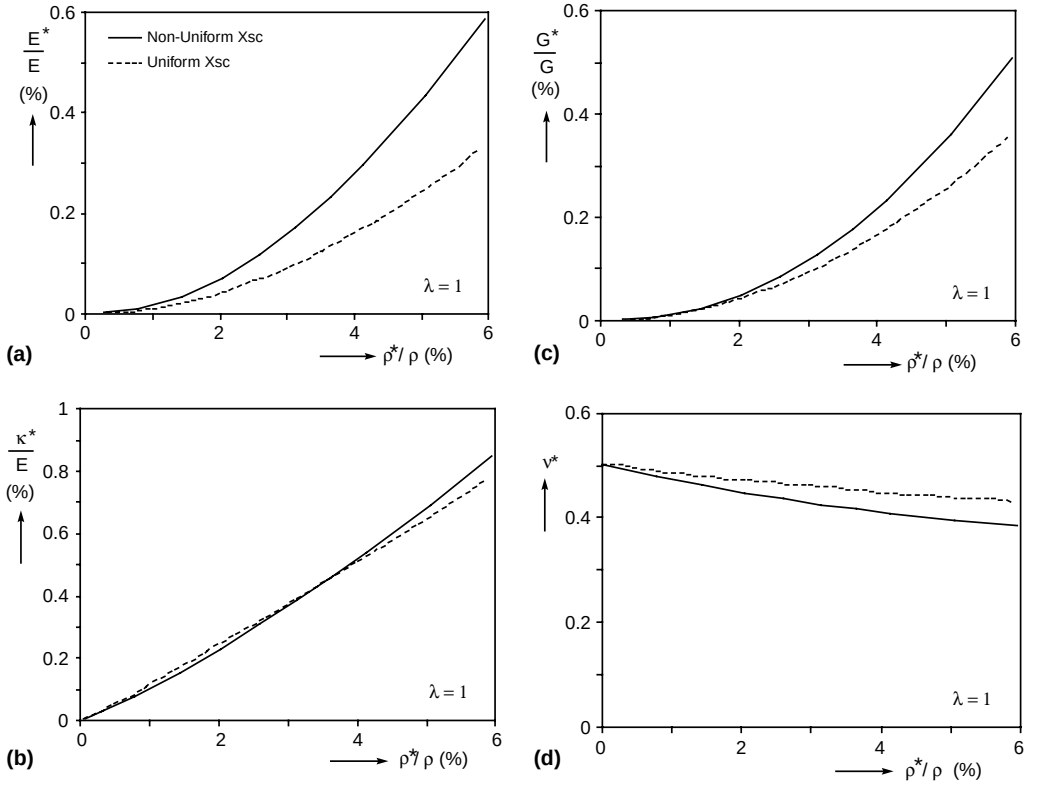

Fig. 19. Material constants vs. relative density for ligaments with uniform and nonuniform cross-sectional areas.

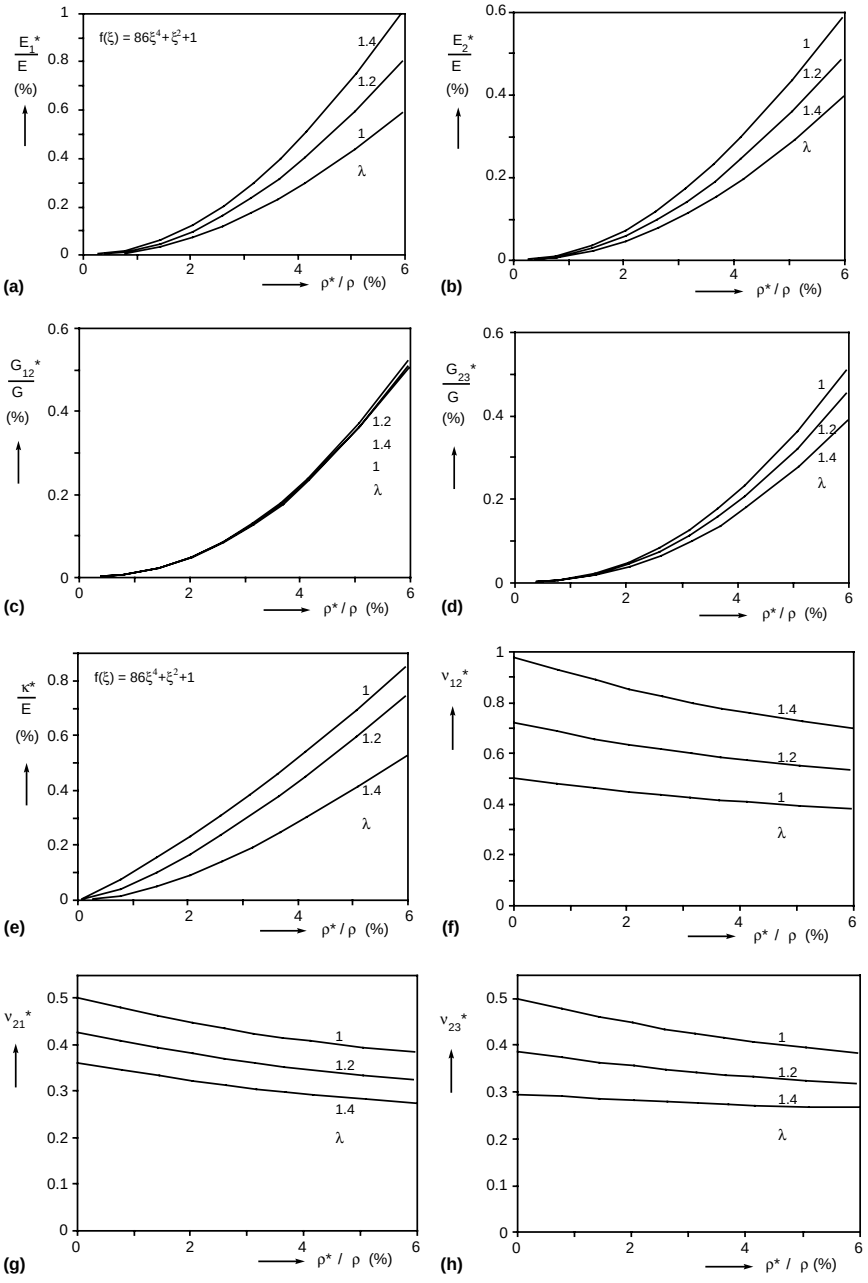

Fig. 20. Material constants vs. relative density for foams with different levels of anisotropy.

(Fig. 20a) while the one in the x_2-direction decreases (Fig. 20b). For example, at a relative density of 3%, λ of 1.2 and 1.4 result in an increase in E_1^* of 36% and 69% respectively and a corresponding decrease in E_2^* of 17% and 35%. The equations in Table 4 show that these changes are directly related to the geometric variable λ.

Table 6
Comparison between measured (E^*_α) and calculated ($\hat{E}^*_\alpha$) elastic moduli foam elastic moduli

Foam ppi	λ	$\frac{\rho^*}{\rho}$ (%)	$\frac{E^*_1}{E}$ (%)	$\frac{\hat{E}^*_1}{E}$ (%)	$\frac{E^*_2}{E}$ (%)	$\frac{\hat{E}^*_2}{E}$ (%)
3	1.432	2.18	0.227	0.152	0.0701	0.0535
10	1.360	2.47	0.181	0.181	0.0707	0.0749
20	1.281	2.36	0.200	0.151	–	0.0747
45	1.256	2.44	0.215	0.156	0.103	0.0819
100	1.233	2.82	0.229	0.203	0.128	0.113

The shear moduli $G^*_{12} = G^*_{13}$ remain unaffected (Fig. 20c) by λ whereas G^*_{23} gets reduced as λ increases (Fig. 20d). Fig. 20e shows that bulk modulus also gets reduced as λ increases. For the isotropic case κ^* is governed by membrane deformations (Table 4). Anisotropy makes κ^* depend also on bending deformations which generally reduce the stiffness. Poisson's ratio v^*_{12} is seen in Table 4 to be proportional to λ^2; as a result it increases significantly with λ as demonstrated in Fig. 20f. By contrast v^*_{21} (Fig. 20g) and v^*_{23} (Fig. 20h) are reduced as λ increases.

Table 6 shows a direct comparison of the measured ($E^*_\alpha, \alpha = 1, 2$) and calculated ($\hat{E}^*_\alpha, \alpha = 1, 2$) values of these moduli using the formulas in Table 4b (including the effect of shear). The predicted moduli are somewhat smaller than the measured values with the biggest difference being 33% for the 3 ppi foam. This favorable comparison suggests that the idealizations made in the geometry of the model foam are reasonable. It also confirms that factors included in the present analysis such as axial and shear deformations, the non-uniformity of the ligament cross-sections and the material distribution at the nodes are essential in getting this level of agreement between measurements and predictions.

5. Summary and conclusions

This study has been concerned with the understanding of the response of open cell foams to uniaxial compression. A set of polyester urethane foams covering a range of cell sizes and with relative densities in the range of 2.2–2.8% were considered. Their microstructures consist of interconnected frameworks forming cells with nearly straight edges. The cells are irregular polyhedra with 9–17 faces. The average number of faces per cell was found to be 13.7. Faces had anywhere from 3 to 7 sides while the average number of sides per face was close to 5. Cells were found to be elongated in the rise direction, a characteristic common to many foams. The anisotropy ranged from $\lambda \approx 1.43$ in the coarser cell foam, to 1.23 in the finer cell one. Because of the way this particular type of foam is manufactured, variation of cell size within each foam was within a relatively narrow range. In addition, the five microstructures were found to scale with cell size (at least to a first order approximation). Cell ligaments have the characteristic three-cusp, Plateau border, cross-section. Their cross-sectional area was found to vary along the length increasing closer to the cell nodes.

Each of the five foams was compressed between rigid plates at prescribed displacement rates. Tests were performed along the rise and transverse directions. Along the rise direction the foams exhibit a force-displacement response shared with many other cellular materials. It starts with a nearly linear elastic regime which terminates into a limit load followed by an extensive load plateau. The plateau is followed by a second branch of stiff response. Because of the cell anisotropy, in the transverse direction the foams were found to be initially more compliant with the modulus being only 1/3 to 1/2 the corresponding values in the rise direction. Surprisingly, the nonlinear part of the response exhibited no load maximum and maintained a monotonically increasing trajectory. The foams are polymeric and, as a result, they exhibit viscoelastic characteristics which have been briefly outlined. Uniaxial tests on single ligaments showed that the base material also exhibits a mild nonlinearity.

A sequence of models for predicting all mechanical foam properties of interest has been developed. The foam is idealized to be periodic using the space filling Kelvin cell assigned the geometric characteristics found in the actual foams. The cells are elongated in the rise direction; the ligaments are assumed to be straight, to have Plateau border cross-sections and nonuniform cross-sectional area distribution. The ligaments are modeled as shear-deformable extensional beams. The base material is assumed to be linearly elastic. A special provision is made to account for the way their intersections at the nodes affect the relative density of the model.

The analytical results in Part I deal with the prediction of the initial elastic moduli of the anisotropic foams. Closed form expressions have been developed for the moduli by analyzing custom microsections. A characteristic cell of the anisotropic microstructure has been established. This was discretized with appropriate shear-deformable beam elements. Numerical results derived from the characteristic cell loaded appropriately, were shown to be in agreement with the analytical expressions for the moduli. The axial moduli of the foams used in the experiments are calculated individually. Comparison between measurements and predictions is very favorable. The paper finishes with results from a limited parametric study of the elastic moduli.

Based on the results presented, it can be concluded that the Kelvin cell model developed is capable of capturing the initial elastic behavior of the foams analyzed. The results also confirm that factors included in the model such as the extensionality and shear deformability of the beam ligaments, modeling of the Plateau border cross-sectional shape and its nonuniformity along the ligament length, and correcting for the material distribution at the nodes are essential in getting this favorable agreement between measurements and predictions. The nonlinear aspects including the crushing behavior of the foams are addressed next in Part II.

Acknowledgments

The financial support of the National Science Foundation through Grant CMS-0245485 and the Air Force Office of Scientific Research through Grant No. F49620-98-1-0145 is acknowledged with thanks. The authors wish to thank Foamex International Inc. for providing foam samples and technical support and Rob Green for conducting several of the foam measurements reported. Special thanks are due to Andy Kraynik of Sandia National Labs for the benefit of technical discussions and exchanges carried out throughout this study.

References

Artavia, L.D., Macosko, C.W., 1994. Polyurethane flexible foam formation. In: Hilyard, N.C., Cunningham, A. (Eds.), Low Density Cellular Plastics: Physical Basis of Behavior. Chapman & Hall, London, pp. 22–55.

Ashby, M.F., Evans, A., Fleck, N.A., Gibson, L.J., Hutchinson, J.W., Wadley, H.N.G., 2000. Metal Foams: A Design Guide. Butterworth-Heinemann.

Choi, J.B., Lakes, R.S., 1995. Analysis of elastic modulus of conventional foams and re-entrant foam materials with negative Poisson's ratio. Int. J. Mech. Sci. 37, 51–59.

Dement'ev, A.G., Tarakanov, O.G., 1970a. Effect of cellular structure on the mechanical properties of plastic foams. Mekhanika Polimerov No. 4, 594–602–865. Translation, pp. 519–525.

Dement'ev, A.G., Tarakanov, O.G., 1970b. Model analysis of the cellular structure of plastic foams of the polyurethane type. Mekhanika Polimerov No. 5, 859–865. Translation, pp.744–749.

Foamex International, Inc., 2003. Personal communication.

Gent, A.N., Thomas, A.G., 1963. Mechanics of foamed elastic materials. Rubber Chem. Technol. 36, 597–610.

Gibson, L.J. (Ed.), 2003. Cellular Solids. MRS Bull. 28/4, 270–306.

Gibson, L.J., Ashby, M.F., 1982. The mechanics of three dimensional cellular materials. Proc. Roy. Soc. Lond. A 382, 43–59.

Gibson, L.J., Ashby, M.F., 1997. Cellular Solids: Structure and Properties, second ed. Cambridge University Press.
Gibson, L.J., Ashby, M.F., Schajer, G.S., Robertson, C.I., 1982. The mechanics of two-dimensional cellular materials. Proc. Roy. Soc. Lond. A 382, 25–42.
Gibson, L.J., Ashby, M.F., Zhang, J., Triantafillou, T.C., 1989. Failure surfaces for cellular materials under multiaxial loads—I. Modeling. Int. J. Mech. Sci. 31, 635–663.
Hilyard, N.C., Cunningham, A. (Eds.), 1994. Low Density Cellular Plastics: Physical Basis of Behavior. Chapman & Hall, London.
Huber, A.T., Gibson, L.J., 1988. Anisotropy in foams. J. Mater. Sci. 23, 3031–3040.
Klintworth, J.W., Stronge, W.J., 1988. Elasto-plastic yield limits and deformation laws for transversely crushed honeycombs. Int. J. Mech. Sci. 30, 273–292.
Kraynik, A.M., 2003. Foam structure: From soap froth to solid foams. MRS Bull. 28/4, 275–278.
Ko, W.L., 1965. Deformations of foamed elastomers. J. Cell. Plastics 1, 45–50.
Laroussi, M., Sab, K., Alaoui, A., 2002. Foam mechanics: Nonlinear response of an elastic 3D-periodic microstructure. Int. J. Solids Struct. 39, 3599–3623.
Matzke, E.B., 1946. The three-dimensional shape of bubbles in foam—An analysis of the role of surface forces in three-dimensional cell shape determination. Amer. J. Botany 33, 58–80.
Menges, G., Knipschild, F., 1975. Estimation of mechanical properties for rigid polyurethane foams. Polym. Eng. Sci. 15, 623–627.
Mullins, L., 1948. Effect of stretching on the properties of rubber. Rubber Chem. Technol. 21, 281–300.
Mullins, L., 1969. Softening of rubber by deformation. Rubber Chem. Technol. 42, 339–362.
Papka, S.D., Kyriakides, S., 1994. In-plane compressive response and crushing of honeycomb. J. Mech. Phys. Solids 42, 1499–1532.
Papka, S.D., Kyriakides, S., 1998a. In-plane crushing of a polycarbonate honeycomb. Int. J. Solids Struct. 35, 239–267.
Papka, S.D., Kyriakides, S., 1998b. Experiments and full-scale numerical simulations of in-plane crushing of a honeycomb. Acta Mater. 46, 2765–2776.
Papka, S.D., Kyriakides, S., 1998c. In-plane crushing of a polycarbonate honeycomb. In: de Borst, R., van der Giessen, E. (Eds.), Proc. IUTAM Symposium Material Instabilities in Solids, June 1997, Delft. Wiley, Chichester, England, pp. 159–183.
Patel, M.R., Finnie, I., 1970. Structural features and mechanical properties of rigid cellular plastics. J. Mater. 5, 909–932.
Plateau, J.A.F., 1873. Statique expérimentale et théorique des liquides soumis aux seules forces moléculaires. 2 Volumes, Gauthier-Villars, Paris.
Pradel, F., 1998. Homogeneisation des milieux discrets periodiques orientes: Une application aux mousses. PhD thesis, Ecole Nationale des Ponts et Chaussees, Camps-sur-Marne.
Priester, R.D., Turner, R.B., 1994. The morphology of flexible polyurethane matrix polymers. In: Hilyard, N.C., Cunningham, A. (Eds.), Low Density Cellular Plastics: Physical Basis of Behavior. Chapman & Hall, London, pp. 78–103.
Shaw, M.C., Sata, T., 1966. The plastic behavior of cellular materials. Int. J. Mech. Sci. 8, 469–478.
Shim, V.P.-W., Stronge, W.J., 1986. Lateral crushing of tightly packed arrays of thin-walled metal tubes. Int. J. Mech. Sci. 28, 709–728.
Thompson, W. (Lord Kelvin), 1887. On the division of space with minimal partitional area. Philos. Mag. 24 (5th Series), 503–514.
Triantafyllidis, N., Schraad, M.W., 1998. Onset of failure in aluminum honeycombs under general in-plane loading. J. Mech. Phys. Solids 46, 1089–1124.
Warren, W.E., Kraynik, A.M., 1997. Linear elastic behavior of a low-density Kelvin foam with open cells. ASME J. Appl. Mech. 64, 787–793.
Warren, W.E., Nielsen, M.K., Kraynik, A.M., 1997. Torsional rigidity of a plateau border. Mech. Res. Commun. 24, 667–672.
Weaire, D., Hutzler, S., 1999. The Physics of Foams. Oxford University Press, Oxford.
Zhu, H.X., Knott, J.F., Mills, N.J., 1997. Analysis of the elastic properties of open-cell foams with tetrakaidecahedral cells. J. Mech. Phys. Solids 45, 319–343.